

Supporting Information

Spin Effects in Regulating the Adsorption Characteristics of Metal Ions

Cunyuan Gao,^{a†} Shiyu Zhen,^{b†} Yutong Wang,^a Lingwei Wang,^a Yang Cao,^a Jinhua Zhan,^a Liang Zhang,^{b,c*} Bin Cai^{a,d*}

^aSchool of Chemistry and Chemical Engineering, Shandong University, 250100 Jinan, China

^bCenter for Combustion Energy, School of Vehicle and Mobility, State Key Laboratory of Automotive Safety and Energy, Tsinghua University, Beijing 100084, China

^cBeijing Huairou Laboratory, Beijing 101400, China

^dShenzhen Research Institute of Shandong University, Shenzhen 518000, China

*Correspondence: bin.cai@sdu.edu.cn; zhangbright@tsinghua.edu.cn

Methods

Chemicals. All chemicals were of analytical grade and used as received. Cobalt acetate tetrahydrate [$\text{Co}(\text{CH}_3\text{COO})_2 \cdot 4\text{H}_2\text{O}$], Zinc acetate dihydrate [$\text{Zn}(\text{CH}_3\text{COO})_2 \cdot 2\text{H}_2\text{O}$], citric acid, acetic (HAc), sodium acetate (NaAc) and ethanol were purchased from Shanghai Mclean Biochemical Technology Co., Ltd. Lead nitrate was purchased from Sinopharm Chemical Reagent Co., Ltd. Acetate buffer solutions of various pH values were prepared by mixing HAc and NaAc solutions. Deionized water was used throughout for preparing aqueous solution.

Apparatus. Electrochemical experiments were carried out using a CHI 760E potentiostat (ChenHua Instruments Co., China) with a standard three electrode system. X-ray diffraction (XRD) was performed on a SmartLab X-ray diffractometer from Rigaku, Japan, employing a Cu X-ray tube operated at a power of 9 KW. Transmission electron microscopy (TEM) analysis was performed on a Tecnai G2 20 (FEI) at an accelerating voltage of 200 kV. The X-ray photoelectron spectroscopy (XPS) spectra were collected on a Thermo Fisher ESCALAB Xi+ with a monochromatic Al K α X-ray source to analyze the element content and valence. For the XPS analysis of Pb^{2+} adsorbed oxide, 10 mg of the oxide powder was suspended with 1 mM Pb^{2+} ions in 10 mL of aqueous solution (0.1 M HAc–NaAc, pH 6.0), and then, the solution was shaken for 24 h. The oxide was then precipitated by centrifugation at 5000 rpm and dried at 60 °C in vacuum for further XPS analysis. Fourier transform infrared spectroscopy (FTIR) data were recorded using FTIR PerkinElmer Spectrum. X-ray absorption spectra (XAS) characterizations were carried out from the Beamlines (XMCD) in Hefei National Synchrotron Radiation Laboratory (NSRL). DC magnetization measurements were performed on a Superconducting Quantum Design (SQUID) magnetometer (MPMS-XL). The SQUID measurements of the magnetization of samples as a function of the magnetic field were carried out at 300 K in fields between -5 T and +5 T. The temperature-dependent magnetizations were measured with a magnetic field (H) of 1000 Oe under field-cooling procedures for all the samples.

Oxides synthesis. Spinel ZnCo_2O_4 oxides were synthesized by a modified conventional sol-gel combustion method. Metal acetates $\text{Zn}(\text{CH}_3\text{COO})_2 \cdot 2\text{H}_2\text{O}$ and $\text{Co}(\text{CH}_3\text{COO})_2 \cdot 4\text{H}_2\text{O}$ with a specific molar ratio were first mixed in dilute nitric acid solution through vigorous stirring.

Citric acid acting as chelating agent, was then added in the mixture. Under the condition of constant stirring at 90 °C for several hours, the mixture solution converts into viscous gel. The gel was then decomposed in air at 170 °C (with a heating rate of 10 °C min⁻¹ to 170 °C) for 12 hours to remove the remaining water and ground thoroughly. After applying a further heat treatment in air at 300 °C, 400 °C, 500 °C, 600 °C (with heating rate of 5 °C min⁻¹) for 6 hours, phase pure spinel oxide powders were obtained.

Computational Details. The geometry optimization and adsorption energies were calculated by DFT calculations via the Vienna ab Initio Simulation package (VASP). The generalized gradient approximation (GGA) in the form of the Perdew-Burke-Ernzerhof (PBE) functional was used to describe the electron exchange and correlation effects. The projector augmented wave (PAW) method was used to describe the interaction between the atomic cores and electrons. A cutoff energy of 450 eV for the plane-wave basis set and an atomic force convergence of 0.02 eV Å⁻¹ were employed. For ZnCo₂O₄, we used DFT+U theory to describe the localized 3d electrons in zinc and cobalt, where $U_{Zn} - J_{Zn} = 4.7$ eV and $U_{Co} - J_{Co} = 3.3$ eV were adopted. ZnCo₂O₄ surface were represent by a four-layer ZnCo₂O₄ (110) slab with a (3×3×1) k-point grid, where the two bottom layers were kept fixed. The slab was separated from its periodic images in the vertical direction by a vacuum space with at least 15 Å. The adsorption energy was calculated according to the equation as follows:

$$E_{ads}(adsorbate) = E(slab + ads) - E(slab) - E(ads)$$

where $E(slab + ads)$, $E(ads)$, and $E(slab)$ are energies of the slab with adsorption, single adsorption, and the clean slab, respectively. The ICOHP analysis was performed by LOBSTER.

Calculation of the lattice distortion of the octahedron. The ZnCo₂O₄ lattices with increased cobalt spin state were adjusted by using the NUPDOWN parameter in VASP, as referenced in Xu's work. We calculated and analyzed the Co–O bond lengths at different spin states and described the lattice distortion using octahedral distortion (ϵ) according to the following expression.

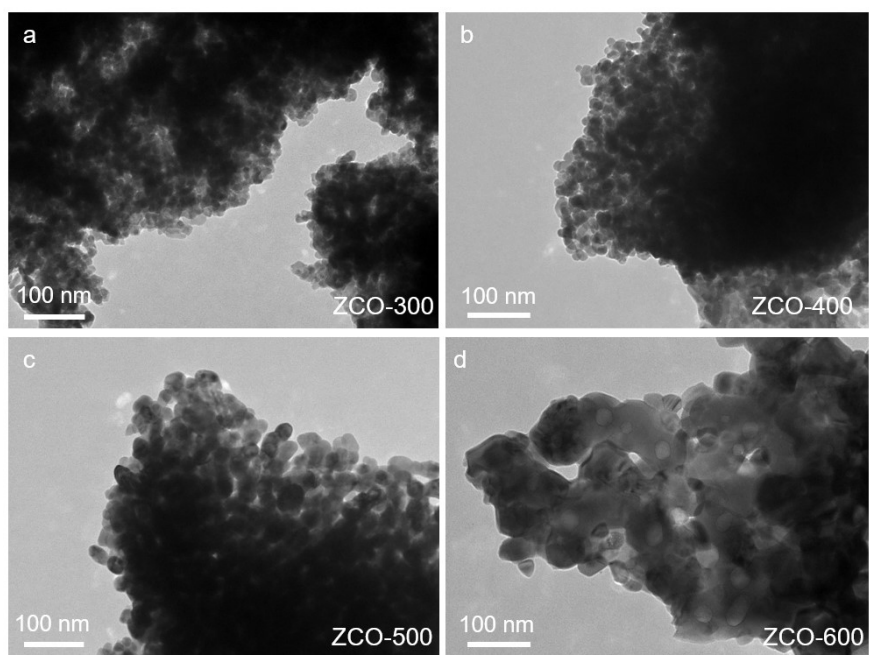
$$\epsilon = \frac{L_{max}}{L_{min}}$$

Where L_{max} represents the maximum Co–O bond length in the octahedron and L_{min} represents

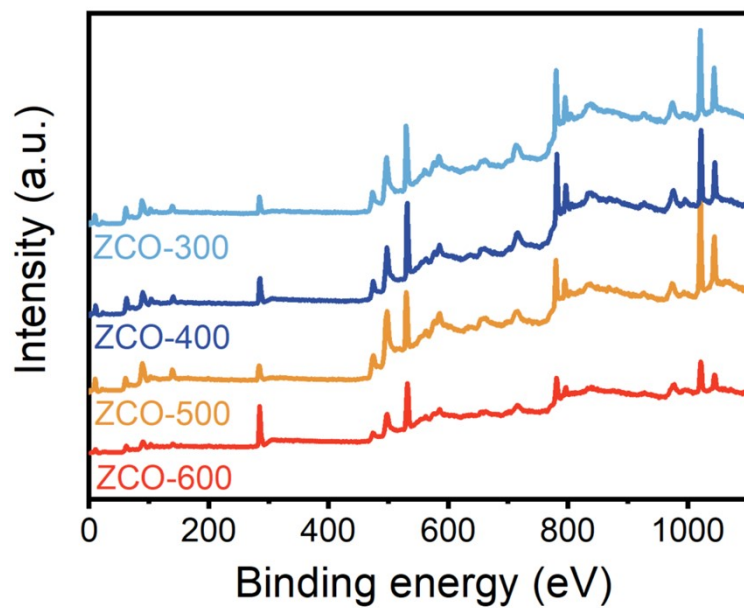
the minimum Co-O bond length in the octahedron

Electrochemical measurements. Electrochemical tests were operated with the glassy carbon electrode (GCE) as the working electrode (3 mm, round), Pt wire as the counter electrode, and Ag/AgCl as the reference electrode. All the GCE was polished with 1.0 and 0.3 μM alumina, followed by sonication in the diluted ethanol. The Spinel oxides were dispersed in ethanol and sonicated for 30 min to form a homogeneous catalyst ink with a concentration of 0.5 mg mL⁻¹. Then, 4 μL of the freshly prepared ink was drop-cast onto the GCE, followed by drying at room temperature. Square wave anodic stripping voltammetry (SWASV) was adopted to detect the target Pb²⁺, Cu²⁺ and Cd²⁺ analyte. The pre-accumulation process was performed at a voltage of -1.0 V vs Ag/AgCl (sat.) for 150 s in 0.1 M HAc-NaAc (pH 6.0), which involves the reduction and deposition of Pb²⁺, Cu²⁺ and Cd²⁺ ion species on the active sites. The anodic stripping was performed at the frequency of 15 Hz, amplitude of 25 mV, and increment potential of 4 mV. After each measurement, the modified electrodes were regenerated by immersing into another fresh 0.1 M HAc-NaAc (pH 6.0) solution under stirring at 1.0 V vs Ag/AgCl (sat.) for 150 s. Cyclic voltammetry and electrochemical impedance spectroscopy (EIS) were performed in 0.1 M KCl containing 5 mM K₃Fe(CN)₆. Besides, the applied potential was set at 0.3 V, frequency range from 1 to 100,000 Hz.

Electrochemical active surface area. The electrochemical active surface area (ECSA) was investigated on the basis of the Randles-Sevcik equation:
$$i_p = 0.4463nFAC\left(\frac{nf\nu D}{RT}\right)^{1/2}$$
, where n is electron number in half-reaction for the redox couple, F is the Faraday constant (96,485 C mol⁻¹), A is the active area (cm²), ν is the sweep rate of potential (V s⁻¹), D is the analyte's diffusion coefficient (cm² s⁻¹), R is the gas constant (8.314 J (mol K)⁻¹), and T is the absolute temperature (K).

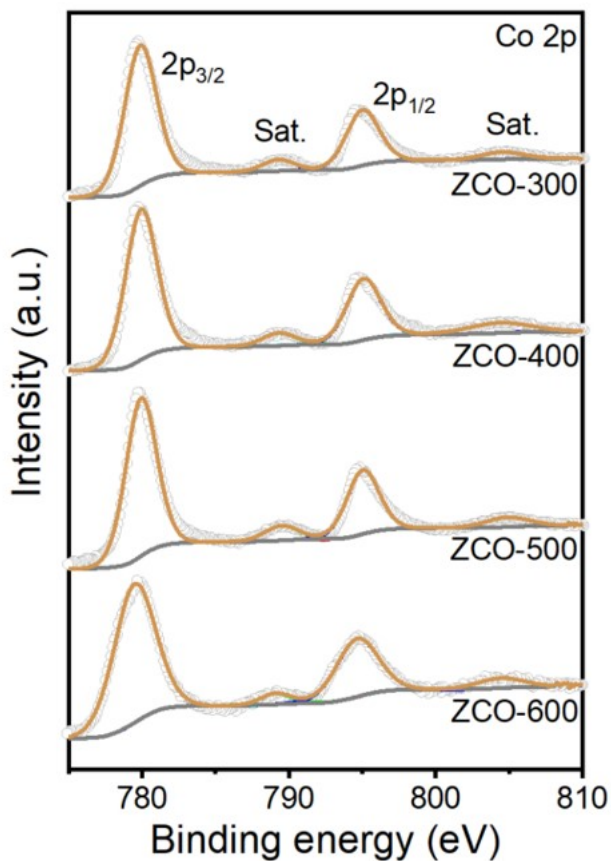


Supplementary Figure 1. Morphological characterization of the ZnCo_2O_4 spinel oxides. TEM images of the as-synthesized (a) ZCO-300, (b) ZCO-400, (c) ZCO-500, (d) ZCO-600.



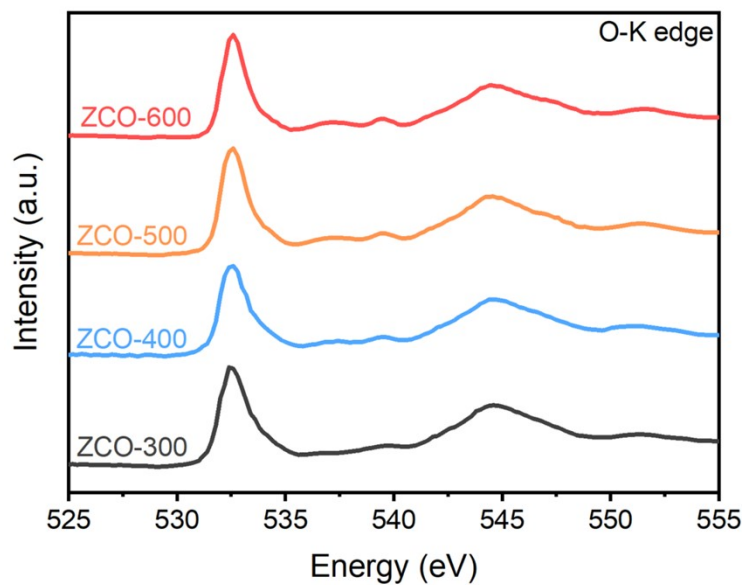
Supplementary Figure 2. Electronic structure characterization of the ZnCo₂O₄ spinel oxides. The XPS general spectrum of the as-prepared ZnCo₂O₄ samples.

The peaks at 800 eV and 1030 eV represent Co 2p and Zn 2p, respectively. It can be seen from the figure that all four samples contain Co and Zn elements.



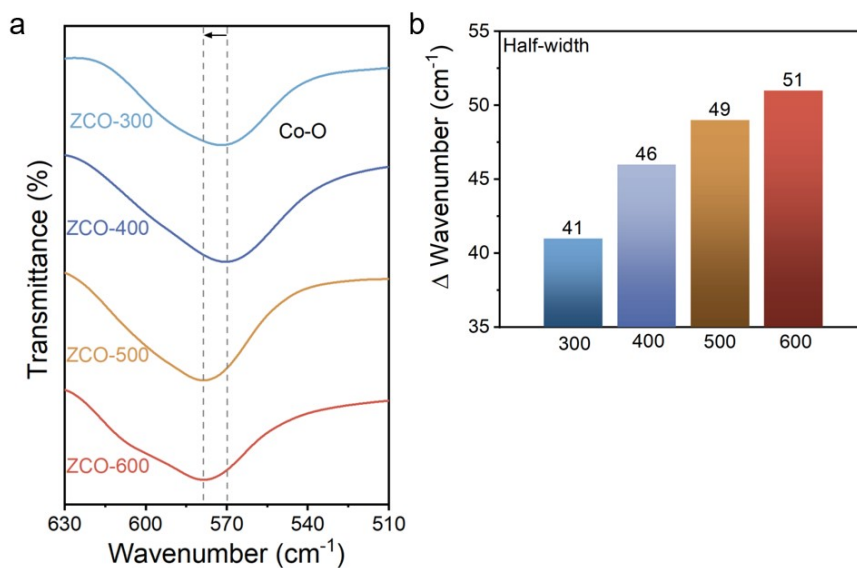
Supplementary Figure 3. Characterization of Co coordination environment. The XPS of Co 2p spectrum of the as-prepared ZnCo_2O_4 samples.

The $2p_{3/2}$ peaks with binding energy at 779.6 eV is assigned to Co^{3+} . In addition to satellite peaks at binding energy of 789.5 and 804.5 eV, the $2p_{1/2}$ peak with lower binding energy (794.7 eV) is indexed to Co^{3+} ions. Therefore, all four synthesized samples have only Co^{3+} octahedral coordination.



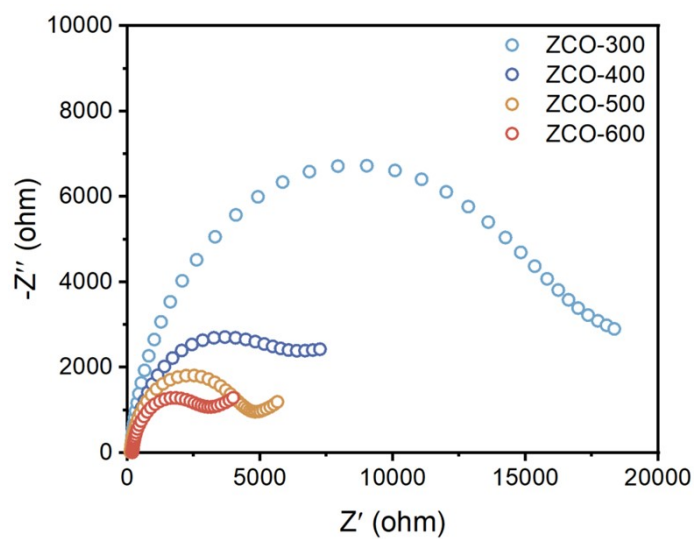
Supplementary Figure 4. The XSA of O-K edge of the as-prepared ZnCo₂O₄ samples.

The peak at 532.5 eV represents O 2p and metal 3d orbital hybridization. The peak at 544.9 eV represents O 2p and metal 4s and 4p orbital hybridization. This indicates a strong coupling interaction between metal and oxygen.

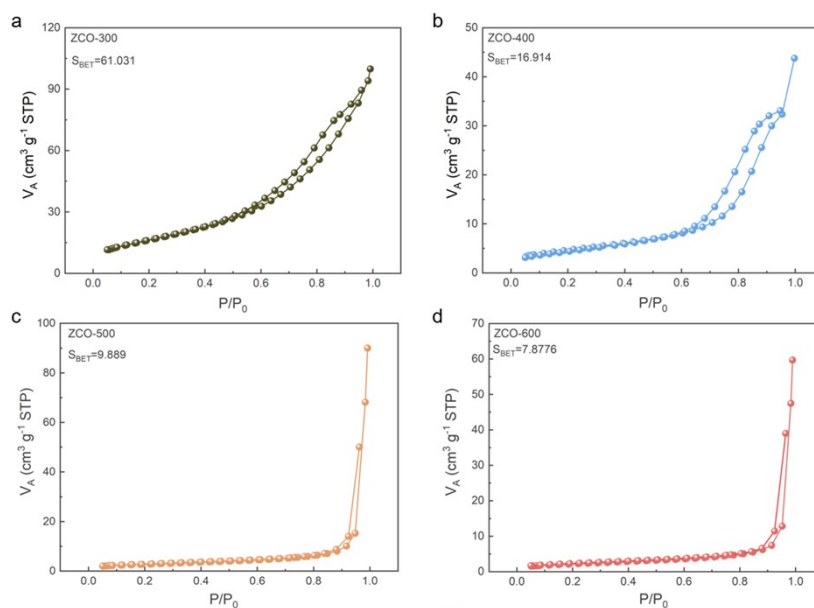


Supplementary Figure 5. Analysis of lattice distortion. (a) FT-IR spectra of the as-prepared spinel ZnCo₂O₄ samples. (b) Comparison of half-width of Co-O vibration peaks of four samples.

As the calcination temperature increases, the peak shape of the M-O bond broadens (from 41 to 51 cm⁻¹) and shifts to higher wavenumber direction, indicating the emergence of lattice distortion.

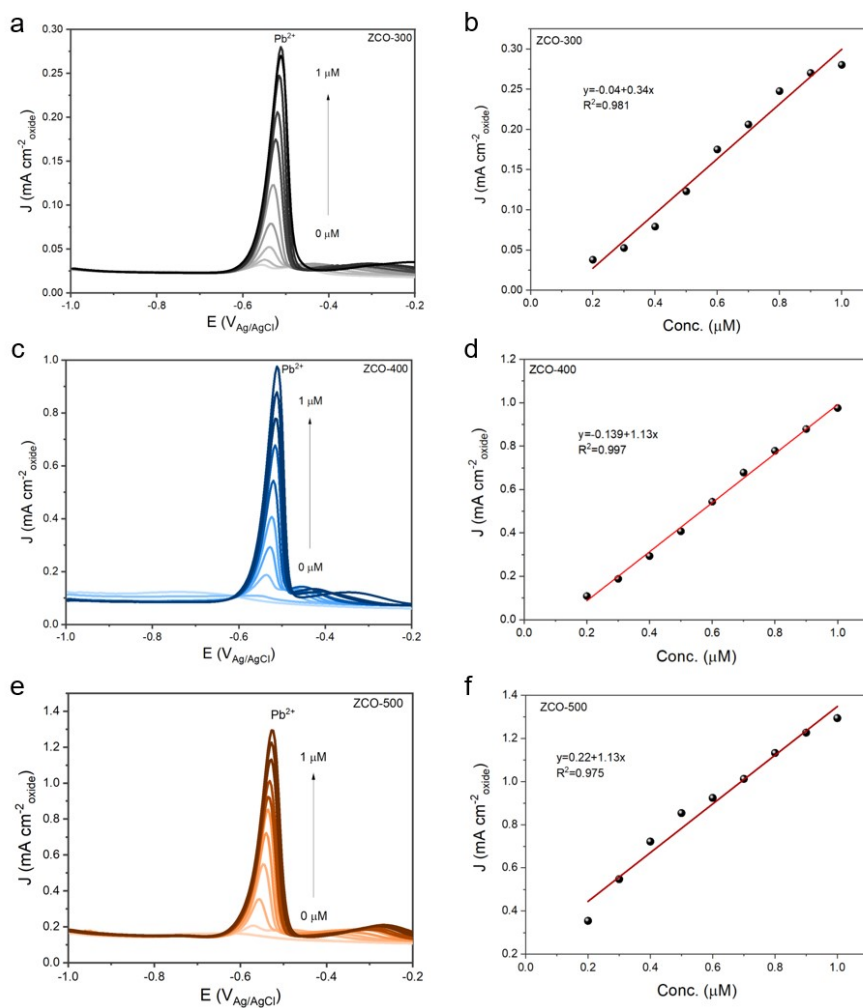


Supplementary Figure 6. The electrochemical impedance spectra (EIS) of the ZnCo₂O₄ spinel oxides.

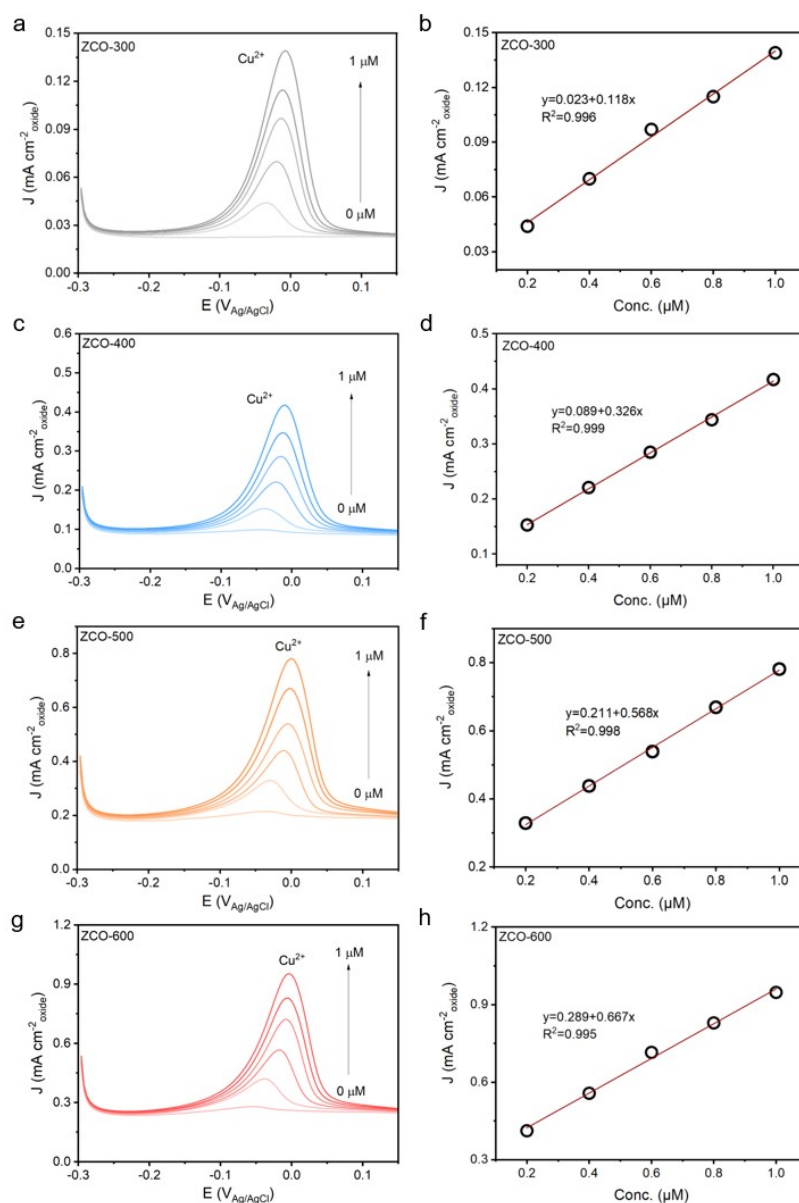


Supplementary Figure 7. Specific surface area characterization. The Brunauer-Emmett-Teller (BET) analysis of the four as-prepared $ZnCo_2O_4$ samples.

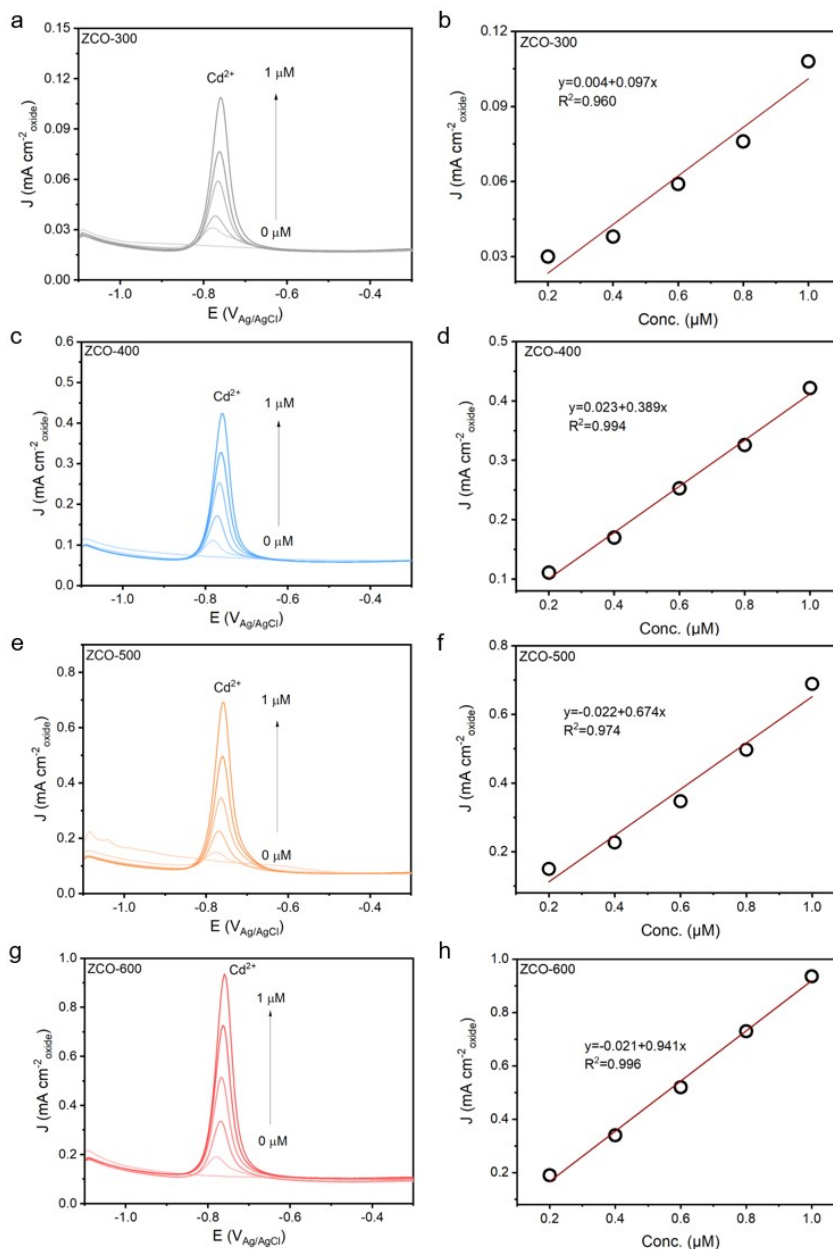
There is N_2 adsorption and desorption isotherm is used to calculate the specific surface area of catalyst. At the relative pressure P/P_0 ranging from 0 to 1 BET isotherm having determination of the overall specific external and internal surface area of nanocomposite. Furthermore, the surface area observed for ZCO-300, ZCO-400, ZCO-500 and ZCO-600 are 61.031, 16.914, 9.889, 7.8776 $m^2 g^{-1}$, respectively.



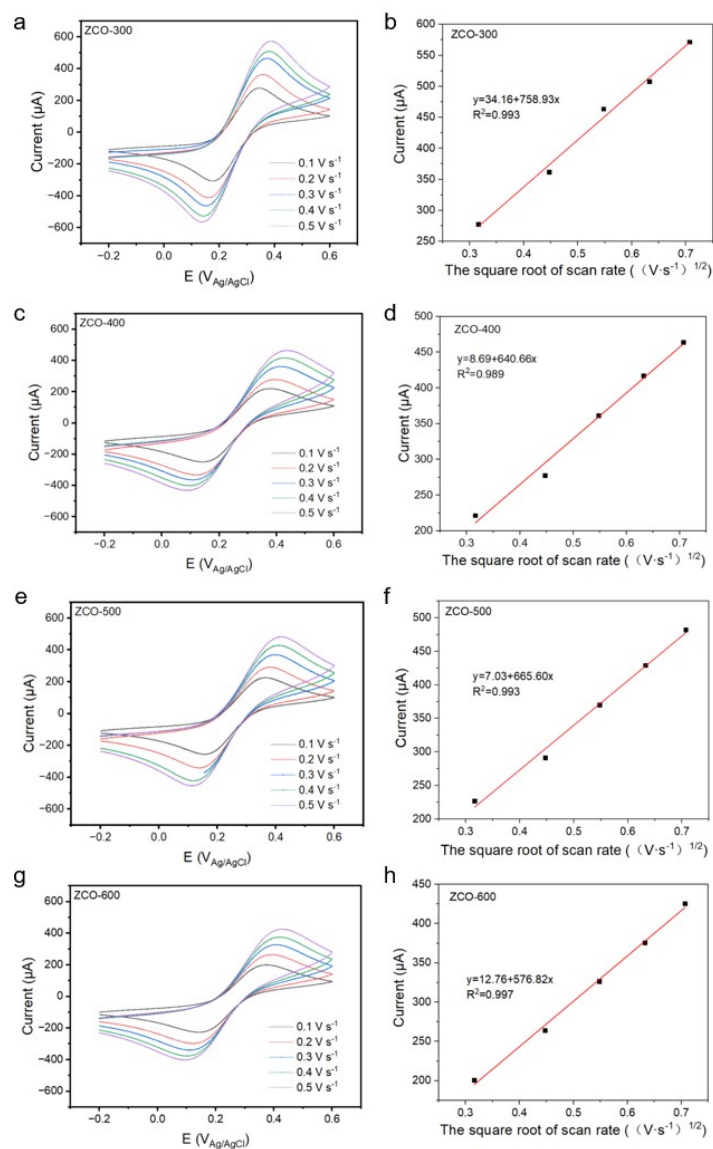
Supplementary Figure 8. Electrochemical detection performance of Pb^{2+} . Typical SWASV responses and corresponding linear calibration plots of samples are as follows: (a, b) ZCO-300; (c, d) ZCO-400; (e-f) ZCO-500 modified GCE toward Pb^{2+} ions. Electrolyte, 0.1 M NaAc-HAc solution; pH = 6.0; deposition potential, -1.0 V vs Ag/AgCl electrode; deposition time, 150 s; amplitude, 25 mV; increment potential, 4 mV; frequency, 25 Hz.



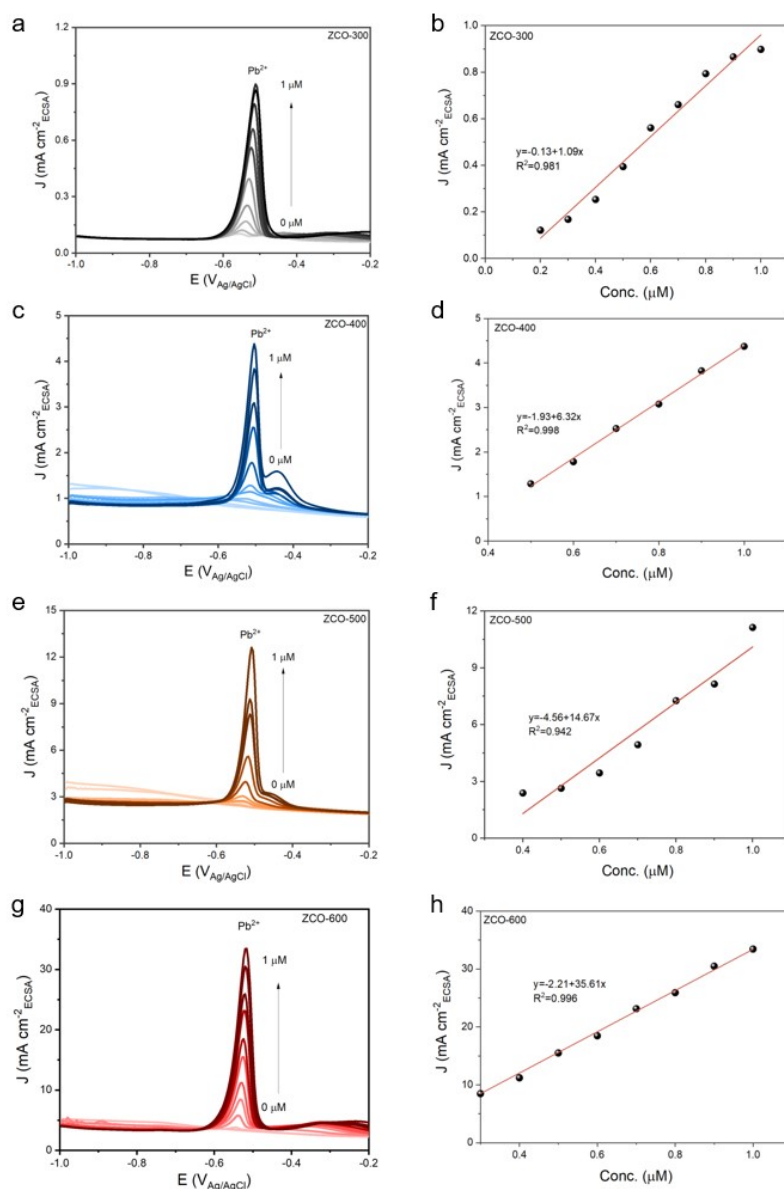
Supplementary Figure 9. Electrochemical detection performance of Cu^{2+} . Typical SWASV responses and corresponding linear calibration plots of samples are as follows: (a, b) ZCO-300; (c, d) ZCO-400; (e-f) ZCO-500; (g-h) ZCO-600 modified GCE toward Cu^{2+} ions. Electrolyte, 0.1 M NaAc-HAc solution; pH = 6.0; deposition potential, -1.0 V vs Ag/AgCl electrode; deposition time, 150 s; amplitude, 25 mV; increment potential, 4 mV; frequency, 25 Hz.



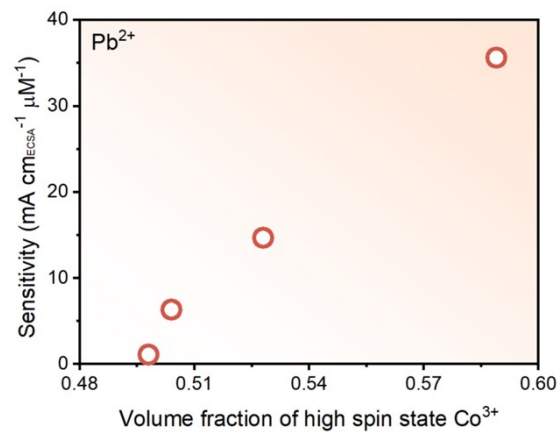
Supplementary Figure 10. Electrochemical detection performance of Cd^{2+} . Typical SWASV responses and corresponding linear calibration plots of samples are as follows: (a, b) ZCO-300; (c, d) ZCO-400; (e-f) ZCO-500; (g-h) ZCO-600 modified GCE toward Cd^{2+} ions. Electrolyte, 0.1 M NaAc-HAc solution; pH = 6.0; deposition potential, -1.0 V vs Ag/AgCl electrode; deposition time, 150 s; amplitude, 25 mV; increment potential, 4 mV; frequency, 25 Hz.



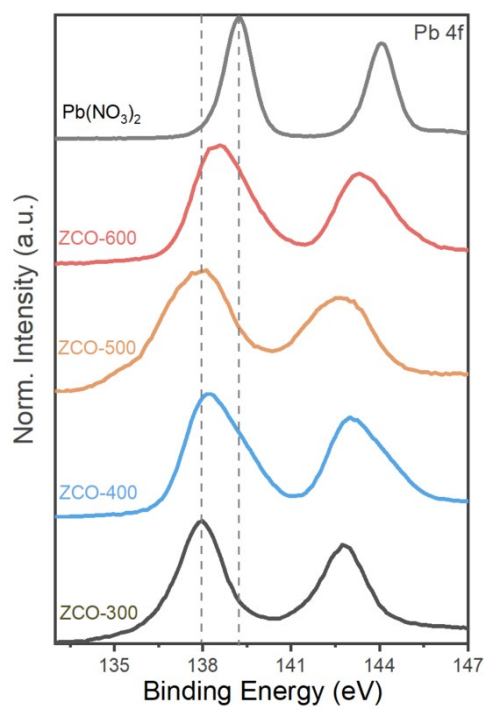
Supplementary Figure 11. Calculation of active area of modified electrodes. (a, c, e, g) Scan rate measurements (from 0.1 to 0.5 V s^{-1}) in the electrolytes of 5 mM $\text{Fe}(\text{CN})_6^{3-/4-}$ containing 0.1 M KCl. (b, d, f, h) The corresponding plots of current vs. the square root of the scan rate with a linear trend line.



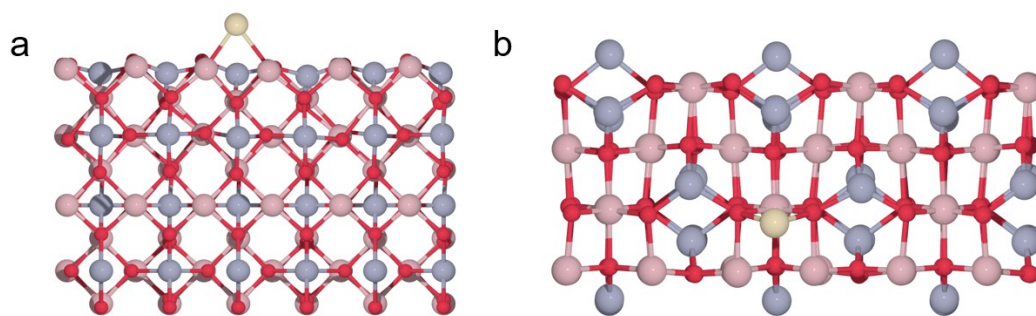
Supplementary Figure 12. Electrochemical detection performance of Pb^{2+} (current density normalized to ECSA). Typical SWASV responses and corresponding linear calibration plots of samples are as follows: (a, b) ZCO-300; (c, d) ZCO-400; (e-f) ZCO-500; (g-h) ZCO-600 modified GCE toward Pb^{2+} ions. Electrolyte, 0.1 M NaAc-HAc solution; pH = 6.0; deposition potential, -1.0 V vs Ag/AgCl electrode; deposition time, 150 s; amplitude, 25 mV; increment potential, 4 mV; frequency, 25 Hz.



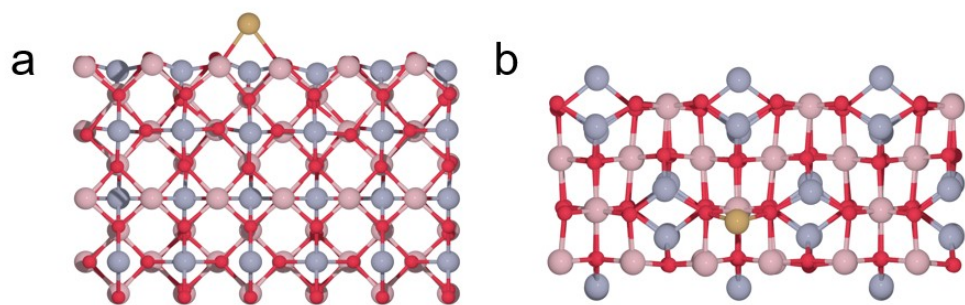
Supplementary Figure 13. Relationship between the volume fraction of high-spin state Co^{3+} and the electrochemical detection sensitivity (current density normalized to ECSA) for Pb^{2+} .



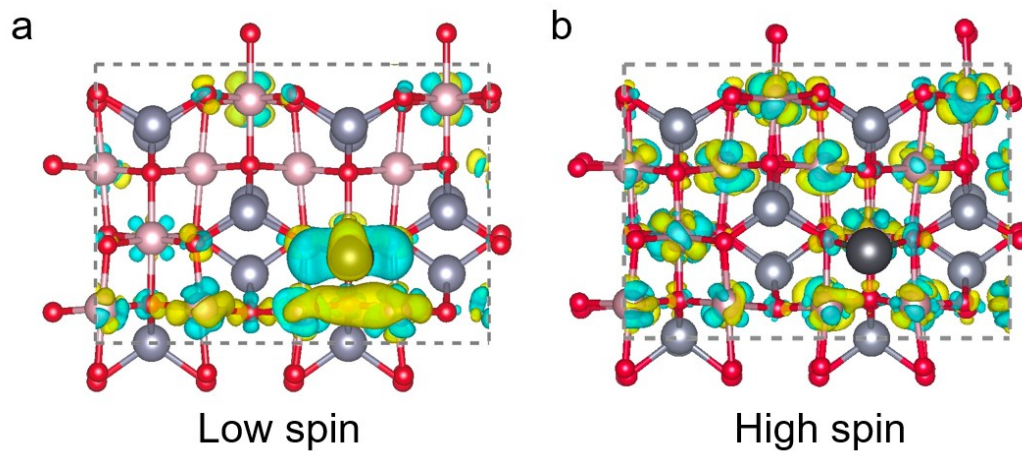
Supplementary Figure 14. Interaction Analysis between ZnCo₂O₄ and Pb²⁺. XPS spectra of Pb 4f after the adsorption of *Pb species for the ZCO-600, ZCO-500, ZCO-400, ZCO-300 and the Pb(NO₃)₂.



Supplementary Figure 15. Side (a) and Top (b) views of the ZnCo_2O_4 models after the adsorption of $^*\text{Cd}$ species. Color scheme: Zn, blue; Co, pink; O, red; Cd, brown.



Supplementary Figure 16. Side (a) and Top (b) views of the ZnCo₂O₄ models after the adsorption of ⁶³Cu species. Color scheme: Zn, blue; Co, pink; O, red; Cu, brown.



Supplementary Figure 17. Top view of differential charge density analysis of (a) low spin, (b) high spin. The blue areas symbolize electron depletion, while the yellow areas symbolize electron accumulation.

Table S1. Curie-Weiss fitting parameters and fitting results of the four as-prepared ZnCo₂O₄ samples.

Samples	ZCO-300	ZCO-400	ZCO-500	ZCO-600
Curie constant	1.50	1.52	1.59	1.77
Spin state	49.8% high-spin + 50.2% low-spin	50.4% high-spin + 49.6% low-spin	52.8% high-spin + 47.2% low-spin	58.9% high-spin + 41.1% low-spin
$\mu_{\text{eff}}(\mu_{\text{B}})$	3.46	3.48	3.56	3.76

Table S2. Comparisons of HMIs detection sensitivity with the four as-prepared ZnCo₂O₄ samples.

	ZCO-300	ZCO-400	ZCO-500	ZCO-600
Pb ²⁺	0.340	0.575	0.982	1.780
Cd ²⁺	0.097	0.393	0.674	0.941
Cu ²⁺	0.118	0.326	0.568	0.667

(Unit: mA cm_{oxide}⁻¹ μM⁻¹)